the frequency. For $l=0$, (4a) leads to the design equation

$$f_p = \frac{C_0}{4s\sqrt{K-1}} \tag{5}$$

where f_p, C_0, s, and K are the frequency for plane wave operation, free-space velocity of light, slab thickness, and relative permittivity, respectively, of the dielectric loading slabs.

Thus over the finite region b by d in^2 and at the particular frequency given by (5), a plane TEM wave traveling in free space can be simulated. Of course, the field distribution over the entire cross section is not TEM since H has an additional axial component within the loading slabs. This component vanishes in the inner-slab vacuum space. The condition for plane waves in region II is independent of the dimensions of region II. Thus, in principle, region II can be made arbitrarily large. As the transverse dimensions are increased, however, there is increasing possibility of the plane wave being distorted by higher order modes. Detailed treatment of higher order modes has been given by Gardiol [4]. Some discrimination against these modes can be achieved by cutting longitudinal slots in the waveguide walls above and below region II; wall currents in this region for the plane wave mode are entirely longitudinal.

The average power flowing in the fields of this "plane wave" mode through a cross section of the structure is

$$P_{av} = \frac{E_0^2}{2\eta_0} b(d+s). \tag{6}$$

The first and second terms of (6) correspond to the average power flowing in the inner-slab space and within the loading slabs, respectively. For $s \ll d$, the power propagating through the dielectric slabs is considerably less than that flowing through the inner space. For the experimental model in Fig. 1, 86 percent and 14 percent of the total power flowed in these two regions, respectively—an important consideration in avoiding dielectric heating and breakdown if the structure must be used in high-power applications.

A dielectric constant of $K=10.07$ for the alumina loading slabs used in the experimental model was calculated using a method based on the shift in the resonant frequency of an iris-coupled TE_{101} rectangular cavity [8]. The waveguide loading slabs were 4.5 in long and were tapered at the ends at an angle of 6.5° over a length of 1 in. The supporting structure consisted of 5 in of reduced height guide tapered at 7° up to standard X-band height. The particular apparatus for which this component was designed required this extended section of reduced height waveguide.

Experimental results for the guide-wavelength measurements versus frequency are presented in Fig. 2. The frequency for which λ_g equals λ_0 was experimentally found to be 8.81 GHz. If $K=10.07$ is used in (5), $f_p=8.76$ GHz results. Inversely, $K=9.94$ in (5) requires $f_p=8.81$ GHz, the experimentally determined value of frequency for plane wave propagation. As these two values of K are within 1 percent, we conclude that (5) has been experimentally verified. Closest agreement was found after the loading slabs were metallized on the three sides that come into contact with the metal waveguide walls.

The magnitude of the electric field is not uniform in the z direction unless the waveguide is propagating a forward traveling wave only. This was achieved by the use of long taper sections from the unloaded waveguide to the loaded waveguide. It should be easier to achieve this using an adjustable load impedance on the output side of the loaded waveguide section.

R. G. Heeren[1]
J. R. Baird[2]
Electro-Physics Lab.
Dep. Elec. Eng.
Univ. Illinois
Urbana, Ill.

References

[1] R. E. Collin, *Field Theory of Guided Waves*. New York: McGraw-Hill, 1960.
[2] L. Young, *Advances in Microwaves*. New York: Academic Press, 1966.
[3] R. F. Harrington, *Time-Harmonic Electromagnetic Fields*. New York: McGraw-Hill, 1961.
[4] F. E. Gardiol, "Higher-order modes in dielectrically loaded rectangular waveguides," *IEEE Trans. Microwave Theory Tech.*, vol. MTT-16, Nov. 1968, pp. 919–924.
[5] R. Seckelmann, "Propagation of TE modes in dielectric loaded waveguides," *IEEE Trans. Microwave Theory Tech.*, vol. MTT-14, Nov. 1966, pp. 518–527.
[6] P. H. Vartanian, W. P. Ayres, and A. L. Helgesson, "Propagation in dielectric slab loaded rectangular waveguide," *IRE Trans. Microwave Theory Tech.*, vol. MTT-6, Apr. 1958, pp. 215–222.
[7] A. Mohsen *et al.*, "Field distribution in multilayered dielectric-loaded rectangular waveguides," *Proc. Inst. Elec. Eng.*, vol. 117, Apr. 1970, pp. 709–712.
[8] M. Sucher and J. Fox, *Handbook of Microwave Measurements*, vol. 2, 3rd ed. Brooklyn, N. Y.: Polytechnic Press, 1963.

Radiation Conductance of Open-Circuit Microstrip

***Abstract*—The radiation conductance of an open-circuit microstrip stub is determined. The losses due to radiation from a stub are shown to be a significant fraction of the total loss.**

Open-circuit microstrip stubs are frequently used in filters and matching networks. An ideal lossless stub with a true open-circuit loading presents a pure susceptance at the junction of the stub and the main line.[1] However, the actual boundary condition at the open end of the line is not an open circuit, but a complex load that can be represented by a conductance G resulting from radiation of the principal mode and a susceptance B resulting from energy stored in the higher order modes. The susceptance B can usually be represented by a hypothetical extension of the stub length of approximately 0.3 to 0.5 substrate thicknesses [1], [2], [3]. Because of the complex load and distributed losses in the stub, the actual stub admittance presented at the junction of the stub and the main line is complex.

In this note, the radiation conductance G at the open end of the stub is determined and used in a calculation of the total losses. The radiation flux is assumed to flow from the open end of the microstrip line directly into the substrate and then finally into the air space above the substrate. Reflection at the dielectric-air boundary is neglected. Under these conditions, G, and consequently the losses, may be found by calculating the radiation from the open end of the stub into the substrate. The calculation will not give information on radiation patterns since the subsequent radiation into the air space is not considered. Some effect of the initial leakage of flux into the air is considered by using Wheeler's [4] effective dielectric constant.

Earlier calculations of G by Marcuvitz [5] and Lewin [6] are applicable to lines with infinitely wide plates and lines with width w much smaller than the guide wavelength λ, respectively. The analysis of this paper covers both cases.

The geometry used in the analysis is shown in Fig. 1. The major assumptions are: (h/λ) is much less than unity; the field distortion near the conductor edge is neglected; the strip conductor is assumed to be infinitely thin; and the only significant contribution to the radiation field is produced by the principal mode electric field at the open circuit.

The electric field E_x in the x-direction is assumed to be a constant E_0 in the space bound by: $-(w/2) \leq z \leq (w/2)$; $-(h/2) \leq x \leq (h/2)$; and zero outside of this region. The fringe field of the line is treated by use of the effective dielectric constant described by Wheeler [4]. Higher order modes resulting in periodic variations in $E_x(z)$ are neglected. Additional assumptions will be described as they are made.

The radiation field can be calculated by a standard method [7]. Maxwell's equations are symmetrized in the aperture (plane of the open circuit) by replacement of the existing electric field by a sheet of virtual magnetic current M that, in turn, is used to calculate a

[1] Now with the School of Engineering, Oakland University, Rochester, Mich. 48063.
[2] Now with the Department of Electrical Engineering, University of Colorado, Boulder, Colo.

Manuscript received December 17, 1970; revised May 5, 1971.
[1] The exact location of the junction will not coincide with the geometric junction, but may be displaced by a distance of the order of the substrate thickness [3].

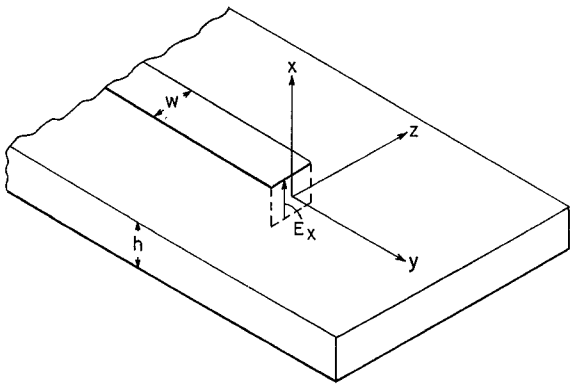

Fig. 1. Geometry for microstrip line.

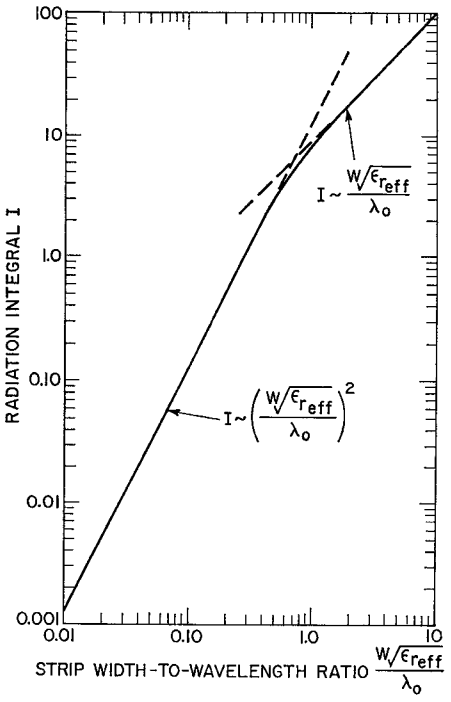

Fig. 2. Integral I as a function of $(w\sqrt{\epsilon_{r_{eff}}}/\lambda_0)$.

magnetic radiation vector L. The only component of magnetic current consistent with the above assumptions is M_x, which leads to a θ-directed magnetic radiation vector L_θ given by

$$L_\theta = -h \sin\theta \int E_x \exp\left[j\frac{2\pi}{\lambda_0}\sqrt{\epsilon_{r_{eff}}}\, z\cos\theta\right] dz. \tag{1}$$

λ_0 is the free-space wavelength and $\epsilon_{r_{eff}}$ is Wheeler's effective dielectric constant. The total radiated power W, and hence G, is given by

$$W = \frac{1}{2}G(hE_0)^2 = \frac{1}{8\lambda^2\eta}\int_0^\pi\int_0^{2\pi} |L_\theta|^2 \sin\theta\, d\phi\, d\theta \tag{2}$$

where

$$\eta = \frac{120\pi}{\sqrt{\epsilon_{r_{eff}}}}.$$

Thus the radiation conductance G is given by

$$G = \frac{\sqrt{\epsilon_{r_{eff}}}}{240\pi^2} I\left(\frac{w}{\lambda_0}\sqrt{\epsilon_{r_{eff}}}\right) \tag{3}$$

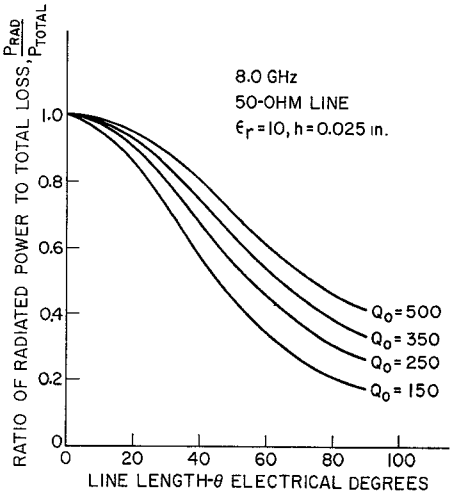

Fig. 3. Ratio of radiation loss to total loss for 50-Ω line as a function of stub length.

where

$$I = \int_0^\pi \frac{\sin^2\left(\frac{\pi\sqrt{\epsilon_{r_{eff}}}}{\lambda_0} w\cos\theta\right)\sin^3\theta}{\cos^2\theta}\, d\theta. \tag{4}$$

Fig. 2 shows the integral I of (4) as a function of $(w/\lambda_0)\sqrt{\epsilon_{r_{eff}}}$. It is to be noted that the conductance varies as $(w/\lambda_0)^2$ for w/λ_0 much less than unity and as w/λ_0 for w/λ_0 much greater than unity, in accord with the earlier work [5], [6].

The integral I can be easily evaluated for $(\pi\sqrt{\epsilon_{r_{eff}}}\, w/\lambda_0)$ much less than unity. For this case, radiation conductance G is given by

$$G \approx \frac{(\epsilon_{r_{eff}})^{3/2}}{180}\left(\frac{w}{\lambda_0}\right)^2. \tag{5}$$

The approximate form of G is quite accurate for $(w/\lambda_0)\sqrt{\epsilon_{r_{eff}}}$ less than 0.5.

The driving point admittance of the stub can be calculated in terms of radiation loading G, the susceptance B, and the distributed line losses expressed in terms of Q_0. The real part g_1 of the driving point admittance, normalized to the stub characteristic admittance, is approximated by

$$g_1 \approx \frac{1}{2Q_0}\frac{\theta\sec^2\theta - \tan\theta + b\tan\theta + b^2(\theta\sec^2\theta + \tan\theta)}{(1 - b\tan\theta)^2} + \frac{g\sec^2\theta}{(1 - b\tan\theta)^2} = g_d + g_r \tag{6}$$

where g and b are the normalized values of G and B, respectively, and θ is the electrical length. The normalized conductance g_d results from the distributed losses, and g_r the radiation losses.

The ratio of the losses that result from radiation to the total stub losses is given by

$$\frac{P_{rad}}{P_{total}} = \frac{g_d}{g_d + g_r}. \tag{7}$$

Fig. 3 shows the ratio (P_{rad}/P_{total}) at 8 GHz plotted for a 50-Ω line on a 0.025-in thick alumina substrate as a function of stub length and illustrates the importance of radiation losses. The value of b used is taken from the results of Napoli and Hughes [2] where the line extension is approximately equal to 0.4 h.

The ratio of the radiation losses to the distributed losses of a quarter wave resonator is given by

$$\frac{P_{rad}}{P_{total} - P_{rad}} = \frac{P_{rad}}{P_{dist}} \approx \frac{Q_0 Z_0 (\epsilon_{r_{eff}})^{3/2}(w/\lambda_0)^2}{45\pi\left(1 + 1.6\frac{h}{\lambda_0}\sqrt{\epsilon_{r_{eff}}}\right)}. \tag{8}$$

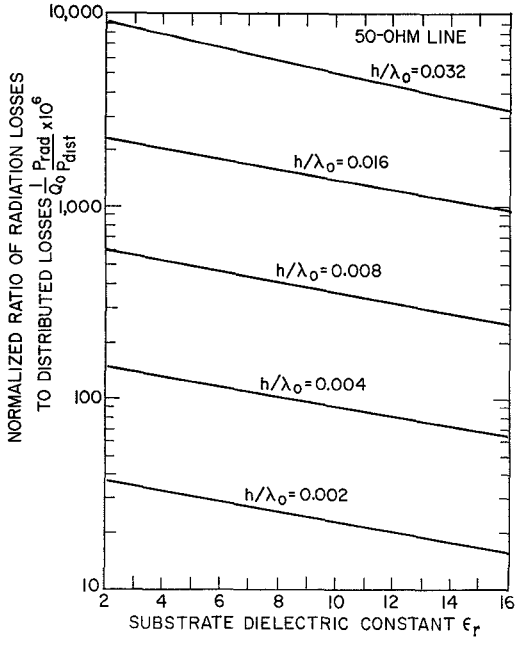

Fig. 4. Ratio of radiation loss to distributed for 50-Ω line as a function of substrate dielectric constant and frequency

Fig. 4 shows P_{rad}/P_{dist} as a function of the substrate dielectric constant ϵ_r and frequency. The results shown are for a 50-Ω line, and are in good agreement with the data presented by Denlinger [8] for radiation losses in excess of 10 percent of the total loss.

H. Sobol
RCA Corp.
David Sarnoff Res. Ctr.
Princeton, N. J. 08540

References

[1] B. R. Hallford, "Low-noise microstrip mixer on a plastic substrate," in *1970 Int. Microwave Symp. Dig.*, pp. 206–211.
[2] L. S. Napoli and J. J. Hughes, "Open-end fringe effect of microstrip lines on alumina," to be published.
[3] H. Stinehelfer, "End effect for microwstrip line," in *Microwave Engineers Technical & Buyers Guide*. Horizon House Microwave Inc., 1969, p. 72.
[4] H. A. Wheeler, "Transmission-line properties of parallel strips separated by a dielectric sheet," *IEEE Trans. Microwave Theory Tech.*, vol. MTT-13, Mar. 1965, pp. 172–185.
[5] N. Marcuvitz, *Waveguide Handbook* (Radiation Laboratory Series, vol 10). New York: McGraw-Hill, 1951, p. 179.
[6] L. Lewin, "Radiation from discontinuities in stripline," *Proc. Inst. Elec. Eng.*, vol. 107, pt. C, Feb. 1960, pp. 163–170.
[7] S. Ramo and J. R. Whinnery, *Fields and Waves in Modern Radio*, 2nd ed. New York: Wiley, 1953, pp. 526–535.
8] E. J. Denlinger, "Radiation from microstrip resonators," *IEEE Trans. Microwave Theory Tech.* (Corresp.), vol. MTT-17, Apr. 1969, pp. 235–236.

Broad-Band Properties of a Class of TEM-Mode Hybrids

***Abstract*—The analysis of a class of *N*-port TEM-mode hybrids, operating as equal or unequal power dividers or summers, has been extended to include the use of tapered transmission lines. The analysis indicates design limitations on the VSWR and isolation characteristics, and can be applied for arbitrary frequency bandwidth and/or power division ratios. Also included are design graphs and tables that cover some common ranges of power division/summation ratios.**

Manuscript received February 19, 1971; revised May 24, 1971. This work was supported in part by the National Research Council of Canada under Grant NRC A-3725.

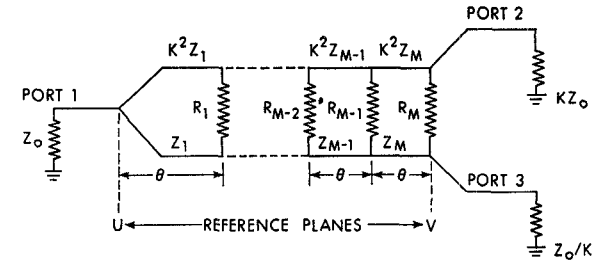

Fig. 1. Circuit for the general case of a three-port hybrid with multiple transformer sections.

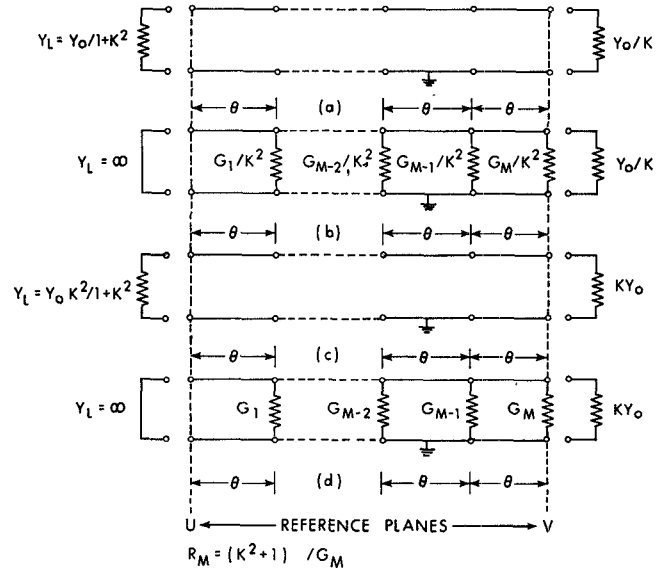

Fig. 2. Even and odd mode equivalent circuits. (a) and (b) Port 1 to port 2 in the even mode and in the odd mode, respectively. (c) and (d) Port 1 to port 3 in the even mode and in the odd mode, respectively.

Introduction

The hybrids to be discussed can be designed for arbitrary power division ratios while maintaining equal phase in the divided parts of the circuit. By the reciprocal properties of this hybrid, signals of equal phase, having given power ratios can also be summed without loss. The summation ports are well isolated from each other within the design frequency band. The work reported here extends that reported previously [1]–[5] to include the use of tapered transmission lines and of distributed resistances to provide the needed impedance matching and isolation. Goodman [6] has given experimental evidence which indicates that it is possible and desirable to use tapered transmission lines in these hybrids. The work discussed here confirms his findings and indicates as well practical values of the distributed resistances to be used.

General Analysis

For analysis purposes, the *N*-port hybrid can be reduced to a four-port equivalent circuit similar to that used for treating the three-port hybrid, as shown in the Appendix. This permits the properties of the hybrid to be readily obtained using the concept of even and odd modes [5].

The general circuit for the three-port hybrid discussed is shown in Figs. 1 and 2 [2], [3]. The basic circuit consists of M sections with an equal number of shunt resistors. The characteristic impedances of the matching sections in each arm serve as impedance transformers to match the summation ports (2 and 3) to the divider port (1). Let the electrical length (θ) be very small, and assume that the characteristic impedance of each increment of length is a stepwise approximation of the tapered transmission line. The shunt resistances can be thought of as the internal termination of the series port, of a conventional four-